



## Analysis of deflection and dynamic plant characteristics of *Cyperus malaccensis* Lam

Mana Shioya, Arata Myoga, Atsuya Kitagawa, Yukihiisa Tokunaga, Hiroaki Hayashi, Yasuo Kogo, Hiroaki Shimada & Shin-ichi Satake

To cite this article: Mana Shioya, Arata Myoga, Atsuya Kitagawa, Yukihiisa Tokunaga, Hiroaki Hayashi, Yasuo Kogo, Hiroaki Shimada & Shin-ichi Satake (2019) Analysis of deflection and dynamic plant characteristics of *Cyperus malaccensis* Lam, Plant Production Science, 22:2, 242-249, DOI: [10.1080/1343943X.2019.1588075](https://doi.org/10.1080/1343943X.2019.1588075)

To link to this article: <https://doi.org/10.1080/1343943X.2019.1588075>



© 2019 The Author(s). Published by Informa UK Limited, trading as Taylor & Francis Group.



Published online: 17 Mar 2019.



Submit your article to this journal [↗](#)



Article views: 524



View related articles [↗](#)



Citing articles: 1 View citing articles [↗](#)

## Analysis of deflection and dynamic plant characteristics of *Cyperus malaccensis* Lam

Mana Shioya<sup>a</sup>, Arata Myoga<sup>a</sup>, Atsuya Kitagawa<sup>a</sup>, Yukihiisa Tokunaga<sup>a</sup>, Hiroaki Hayashi<sup>b</sup>, Yasuo Kogo<sup>c</sup>, Hiroaki Shimada<sup>d</sup> and Shin-ichi Satake<sup>a</sup>

<sup>a</sup>Department of Applied Electronics, Tokyo University of Science, Tokyo, Japan; <sup>b</sup>Hayashi Farm, Kunisaki City, Oita, Japan; <sup>c</sup>Department of Materials Science and Technology, Tokyo University of Science, Tokyo, Japan; <sup>d</sup>Department of Biological Science and Technology, Tokyo University of Science, Tokyo, Japan

### ABSTRACT

In this study, flexural rigidity, natural frequency, and damping coefficient of *Cyperus malaccensis* Lam. with long stems were measured for application for fluid–structure interaction simulation in a field. Numerical solutions of deflection and natural frequency were calculated by ANSYS with finite element method (FEM). The triangular cross-section shape of *C. malaccensis* stem has a big neighbourhood of the root and the cross-section has taper structure to become small towards tip direction. Two numerical simulation models for FEM have Model A with a triangular prism shape and Model B with a truncated trigonal pyramidal shape to evaluate the effects of stem tapering. Because of large *C. malaccensis* stem deflection, an equation for nonlinear deflection was introduced to solve a problem regarding flexural rigidity. Natural frequencies of the stem were estimated using amplitude ratio during stem swinging by forced vibration, captured using a high-speed camera. The Model B corresponded with the measurement, and the results suggested that the stem characteristics were affected by cross-section shape. Damping coefficient was calculated using free vibration response, which was consistent with the analytical solution and numerical data calculated using measured characteristics.

**Abbreviations:** *C. malaccensis*: *Cyperus malaccensis*; FEM: finite element method; GIAHS: Globally Important Agricultural Heritage System

### ARTICLE HISTORY

Received 19 April 2018  
Revised 15 January 2019  
Accepted 21 February 2019

### KEYWORDS

*Cyperus malaccensis* Lam; deflection; frequency response; finite element method; forced vibration experiment

## 1. Introduction

*Cyperus malaccensis* Lam. (Order, Cyperales; Family, Cyperaceae) is a sedge, commonly called the Chair Maker or Chinese Matgrass. This plant serves as the raw material for making tatami mats and is cultivated mainly in Japan and China (Hayashi, 2014). In Japan, it is cultivated only in the Kunisaki Peninsula, owing to its time-consuming cultivation and high-quality imported goods. After the Kunisaki Peninsula was registered as a Globally Important Agricultural Heritage System (GIAHS) as the 'Kunisaki Peninsula Usa Integrated Forestry, Agriculture and Fisheries System' by the Food and Agricultural Organization of the United Nations at 2013, *C. malaccensis* has again come under the global attention as an important industrial fiber crop (Hayashi, 2014). The characteristics of *C. malaccensis* are its sharp, triangular and long stem, absence of nodes, and 2–3 leaves at the stem tip (Karamchand et al., 2009). It is harvested when it reaches a height of ~1.5 m after its stem has been cut several times to ensure uniform stem thickness.

The properties of the fibers, such as the length, elasticity, and number density, affect the flow structure in the canopy layer. The oscillation amplitude of the fibers increases with appropriate fiber properties and flow conditions (Murakami, Harazono, Kawamura & Nishizawa, 1990). This indicates that a canopy can be used to control the flow, exchange of heat, and mass transfer in the canopy. To detect the optimal conditions of length and number density for the plant, numerical simulation is useful without an experiment in paddy fields. For example, numerical simulation investigates the interactions between the turbulent flow and elastic fibers (Hanawa, Miyauchi, Takeuchi & Kajishima, 2015). In one study, a parameter study was conducted to investigate the effects of the properties of fibers, such as the length, elasticity, and number density, on the turbulent flow. They showed that the effects of the fiber properties on the interaction between the turbulent flow and the numerical simulation can obtain fibers implanted on a flat plate. Therefore, numerical simulation enables us to predict the interaction between the turbulent flow and

crops in paddy field if a real plant's properties are provided as simulation parameters (the stem length, interval of crops, etc.). The plants have been observed to become deformed with the flow of air and water (Vogel, 1984). Unique phenomena, such as honami and monami, caused by the organized structure of plant canopies and fluid–structure interactions, have been reported (Inoue, 1963). In various plants, investigation of these phenomena has been attempted as a numerical solution to problems about fluid–structure interactions (Dupont, Gosselin & Py et al., 2010). These are affected by the stiffness and vibration characteristics of the plant (Baker, 1995; Martinez-Vazquez & Sterling, 2011). The natural frequency,  $f$  (Hz), and damping coefficient,  $\xi$ , as a numerical parameter are necessary to perform the simulation. Our objective is the simulation of cultivated fields with *C. malaccensis* stems to improve the cultivation efficiency (e.g. interval of crops). To perform the simulation, we firstly needed the properties of *C. malaccensis* stems as the numerical parameter. However, these characteristics of *C. malaccensis* stems have not yet been described in detail.

In this study, we attempt to determine the *C. malaccensis* stem characteristics, including flexural rigidity, natural frequency, and damping coefficient, from experimental data. Flexural rigidity  $EI$  (N/m<sup>2</sup>) was calculated from deflection, measured by applying a load at the top of the stem. Natural frequency  $f$  (Hz) was determined through a forced vibration experiment. In a natural damping experiment, damping coefficient  $\xi$  and natural frequency at damping vibration  $f_D$  (Hz) were determined from the free damping response.  $f_D$  was compared with  $f$ . To confirm that the measured  $EI$  estimated the characteristics, two types of models were constructed and solved by ANSYS, a software package for solving problems numerically using the finite element method (FEM). The number of plant samples used in the experiments and calculations was 20.

## 2. Materials and methods

### 2.1. *C. malaccensis* plant material

*C. malaccensis* is cultivated in paddy fields, with Haplic Gray Lowland soils according to Cultivated Soil Classification Committee (1995), located at latitude 33°32'N, longitude 131°37'E and 192 m above sea level in Oita Prefecture, the Northeast Kyusyu Island, Japan as shown in Figure 1. A commercially available, compound chemical fertilizer (EMCOTE522, Ryotou Hiryo Co., Ltd., Oita, Japan) was applied as the basal dressing at 390.0 kg N ha<sup>-1</sup>, 136.2 kg P ha<sup>-1</sup>, and 258.9 kg K ha<sup>-1</sup>. *C. malaccensis* seedlings were planted in watered paddy fields at a density of 14.7 seedlings m<sup>-2</sup> on 20 May 2017 and harvested on

27 July 2017. Harvested stems with minimum roots (Figure 2) were transferred to the laboratory of Tokyo University of Science at 6-3-1 Nijuku, Katsushika-ku, Tokyo and then necessary measurements were carried out 6 h after they were harvested.

*C. malaccensis* has a sharp, triangular and long stem without nodes and with 2–3 leaves at the tip of the stem. The leaf mass is so small that their ability of motion can be ignored. Leaves and roots were cut from the stem prior to the following experiments. Cross-sections of the stem are shown in Figure 3. Figure 3(a) indicates the region near the root; Figure 3 (b–g) indicate positions at increasing distances of 15 cm from Figure 3(a), and Figure 3(h) indicates the stem top where leaves grow.

### 2.2. Forced vibration experiment and natural frequency

The vibrator system is shown in Figure 4. It was composed of a brushless motor (BLM460S-GFV2; Oriental Motor Co., Ltd.), bearings, and sliding rails. Rotational motion of the motor was converted by the bearings and sliding rails into horizontal oscillatory motion. The rotational frequency of the motor was dampened by a gear (GFV4G5; Oriental Motor Co., Ltd.) to 16–800 rpm. The frequency range that could be measured by the system was 0.27–13.33 Hz. The slider stroke was 1.0 cm long (amplitude of 0.5 cm).

The stem of *C. malaccensis* was fixed vertically onto a plate fitted with sliders and bearings. The swinging motion of the stem was recorded with markers for scale using a high-speed camera (NX5-S2, Integrated Device Technology Inc.). During the measurement, the forced frequency was 0.02 Hz around the amplitude peak and 0.2 Hz at other points from 0.4 Hz to 3.0 Hz. Frame rates were set as 500–4000 fps, as there were over 1300 frames within the period at each frequency with a resolution of 256 × 256 pixels.  $f$  was estimated at a frequency where the frequency response curve showed a peak. Forced frequency was increased by 0.02 Hz from 0.8 Hz to 1.0 Hz and 0.2 Hz in other, and measured using sample No. 1.

### 2.3. Deflection test and FEM

Deflection of the stem,  $w$ [m], was measured with experimental equipment is shown in Figure 5. Markers, used as reference points, were attached to the wall. The stem was fixed horizontally on the same surface, and a load was applied at the top of the stem with markers as sampling points along the stem.



**Figure 1.** *Cyperus malaccensis* Lam. in a paddy field in the Hayashi farm. It is located at latitude 33° 32'N, longitude 131° 37'E, and 192 m above sea level in Oita Prefecture, northeast Kyusyu Island, Japan.

Stem deflection,  $\omega$  (m), was measured with experimental equipment is shown in Figure 5. Images of markers and the stem were captured using a single-lens reflex camera (D3400 and AF-P DX NIKKOR, Nikon Corporation).  $\omega$  and height [ $y$  (m)], which is the horizontal distance between the fixed base and the top of the stem, were measured from the image. For each sample, there were three cases, i.e. the stem was loaded with 0 g, 1.0 g, and 3.0 g.

Since the stem was easily deformed, its deflection could approach a small linearity deflection. To calculate  $EI$ , equations that could be applied to a large deflection were used. Considering the stem as a horizontally fixed cantilever beam, the equation for moment derived from a theoretical formula (Inoue, Kim, Hashiguchi & Okayasu et al., 1998) was:

$$-\frac{M}{EI} = \frac{\frac{d^2\omega}{dy^2}}{\left\{1 + \left(\frac{d\omega}{dy}\right)^2\right\}^{3/2}} \quad (1)$$

where  $M$  is the bending moment (Nm). It follows from the integrated Equation 1:

$$\frac{d\omega}{dy} = \frac{lx - \frac{y^2}{2}}{\sqrt{\left(\frac{EI}{P}\right)^2 - \left(y - \frac{y^2}{2}\right)^2}} \quad (2)$$

which is a differential equation for deflection angle, where  $l$  (m) is the maximum of  $y$ , and  $P$  (N) is the applied load. Deflection due to the mass of the stem  $\omega_M$  (m) was not considered in Equation 2.  $\omega$  was defined as the difference between  $\omega_M$  and deflection with  $P$  [ $\omega_P$  (m)].  $EI$  was calculated using Simpson's rule because it was difficult to determine the accurate solution of Equation 2.

To confirm that the measured  $EI$  estimated the characters, two types of models were prepared and solved by ANSYS. ANSYS is a software package from ANSYS Inc. for solving problems numerically using the FEM. In this study, a part of the package, which can set detailed parameters to models, ANSYS Mechanical APDL 14.5, was used to estimate deflection and natural frequency using the finite element model.

Two types of models were proposed (Figure 6). Figure 6(a) is Model A with triangular prism shape. In Model B, we considered the taper section that we acquired to get closer to the cross-section of the real plant (see Figure 3).

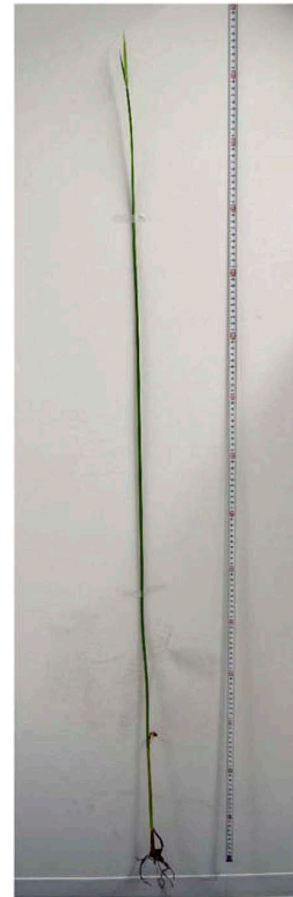


**Figure 2.** A harvested *C. malaccensis* stem with roots. The stems were transported to the laboratory of the Tokyo University of Science at 6-3-1 Nijuku, Katsushika-ku, Tokyo, and the necessary analyses were conducted 6 h after the harvest.

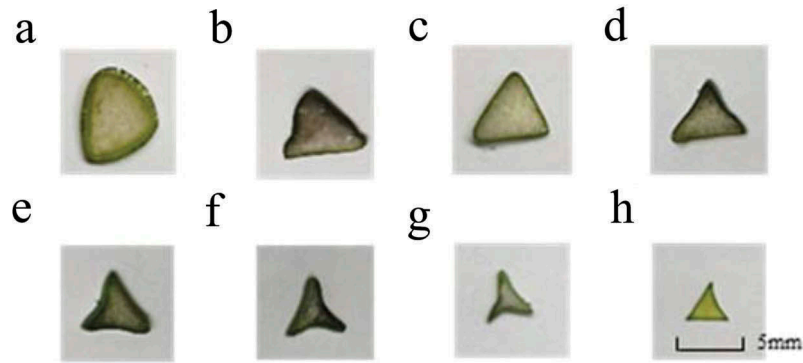


**Figure 3.** Cross-sections of *C. malaccensis* stem. (a) indicates the region near the root; (b–g) indicate positions at increasing multiples of 15 cm from A, and (h) indicates the stem top where the leaves grew.

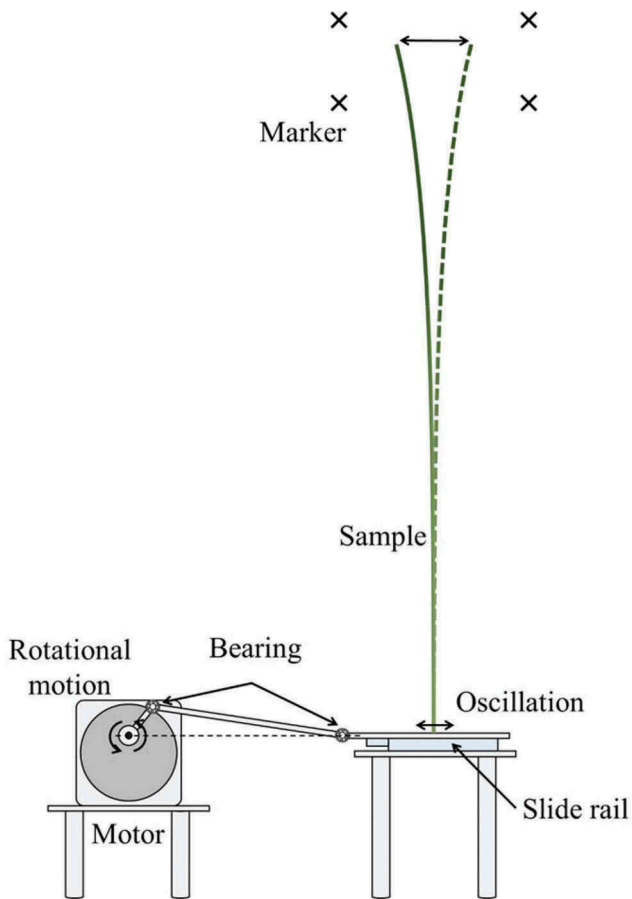


**Figure 4.** Experimental system for the forced vibration experiment. It was composed of a brushless motor (BLM460S-GFV2; Oriental Motor Co., Ltd.), bearings, and sliding rails. Rotational motion of the motor was converted by the bearings and sliding rails into horizontal oscillatory motion. The rotational frequency of the motor was dampened by a gear (GFV4G5; Oriental Motor Co., Ltd.) to 16–800 rpm. The frequency range that could be measured by the system was 0.27–13.33 Hz. The slider stroke was 1.0 cm long (amplitude: 0.5 cm).

**Figure 6(b)** is Model B with truncated trigonal pyramidal shape. Mesh sizes along the length were 0.0012–0.0016 m in Model A and 0.0016 m in Model

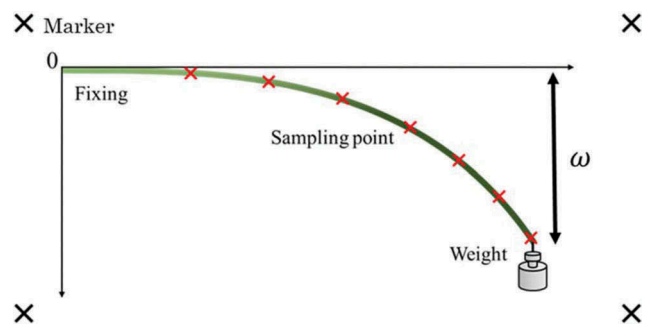


**Figure 5.** Measuring system for the deflection test. Markers, used as reference points, were attached to the wall. The stem was fixed horizontally onto the same surface, and a load was applied to the top of the stem with markers as sampling points along the stem.

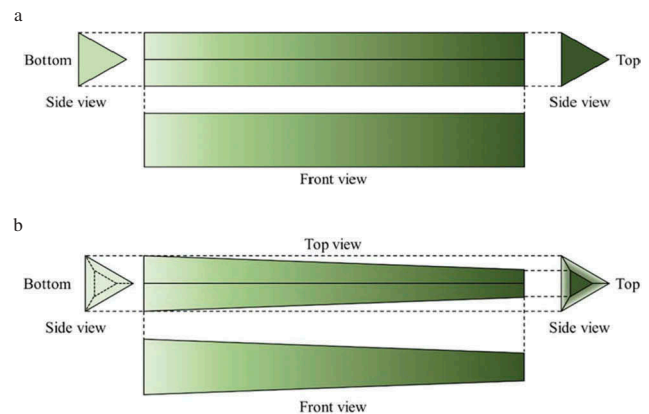


**Figure 6.** Finite element models. (a) Model A with a triangular prism shape. (b) Model B with a truncated trigonal pyramidal shape.

B. Each cross-section was divided into 12 parts in both models. The models were solved as three-dimensional linear elastic analysis. Their elements were first-order and mapped hexahedron type.

In Model B, the moment of inertia of area  $I$  depended on the region along its length. Young's

modulus of Model B,  $E_B$ , was defined as  $EI/\bar{I}$ , where  $\bar{I}$  is the average moment of inertia of the area along the length direction of Model B.

The stem of *C. malaccensis* is tapered in its growth stage. The tapered stem is cut several times to widen it before harvesting. This study focused on growing plants with tapering stems. To consider the effect of shape on the deflection wave, tapered Model B as well as flat model A were constructed and compared. Since the deformation of these models was predicted to increase, the option large displacement static in ANSYS was selected.

Natural frequencies were calculated using Model A  $f_A$  and Model B  $f_B$ . Block Lanczos algorithm was selected as the mode extraction method in modal analysis by ANSYS.

**2.4. Natural damping experiment and FEM**

The stem was fixed vertically on the plate, pulled from its position of static equilibrium to ~10 cm away, and released gently. The swinging motion was recorded with markers for scale using the high-speed camera (NX5-S2, Integrated Device Technology, Inc.). The frame rate was 2000 fps, with a resolution of 256 × 256 pixels.

If the horizontal displacements from the static position to the first peak and second peak of damping motion are  $x_0$  and  $x_1$ , respectively, the amplitude ratio of damping is given by Flesch and Grant (1992):

$$\frac{x_0}{x_1} = \exp\left[2\pi\xi(1 - \xi^2)^{\frac{1}{2}}\right]. \tag{3}$$

$x_0/x_1$  is calculated using  $\xi$  only. By rearranging Equation 3 for  $\xi$ , the following equation,

$$\xi = \sqrt{\frac{1}{1 + \left(\frac{2\pi}{\ln(x_0/x_1)}\right)^2}}, \tag{4}$$

is obtained. This equation implies that  $\xi$  can be calculated using the measured damping curve.  $f_D$  is defined as:

$$f_D = \frac{1}{(t_1 - t_0)\sqrt{1 - \xi^2}} \tag{5}$$

where  $t_0$  is the time at  $x_0$ , and  $t_1$  is the time at  $x_1$ . To introduce the measured displacement and time into Equations 4 and 5,  $\xi$  and  $f_D$  were determined.

We used the Newmark- $\beta$  method as the numerical method for solving the differential equations. It is a method of numerical integration for solving equations that include an irregular external force (Newmark, 1959).  $\beta$  is selected by assuming variation in acceleration. In this study,  $\beta$  was 1/8.

**3. Results**

**3.1. Characteristics of marital plants**

The characteristics of *C. malaccensis* evaluated in this study are shown in Table 1. Water content was estimated from dry mass by desiccating the well at room temperature.

$d$  is the average side length of the cross-section of the stem, assumed to be triangular.  $d_b$  and  $d_t$  are the lengths at the base and top of the stem, respectively. The coefficient of variation of water content was smaller than those of the other parameters.

**Table 1.** Characteristics of *Cyperus malaccensis* Lam. evaluated using 20 plant samples.

Plant number	$L$ (m)	$d_b$ (m)	$d_t$ (m)	Mass (kg)	$EI$ (Nm <sup>2</sup> ) (load 1.0 g)	$EI$ (Nm <sup>2</sup> ) (load 3.0 g)	$F$ (Hz) (forced exp.)	$f_D$ (Hz) (natural damping exp.)	$f_A$ (Hz) (Model A)	$f_B$ (Hz) (Model B)	Damping coefficient	Water content (%)
1	1.242	0.00604	0.00307	0.0109596	0.017166	0.017850	0.98	0.9598	0.54905	0.9279	0.0517	84.533
2	1.311	0.00573	0.00272	0.0106624	0.017229	0.013635	0.90	0.9201	0.45038	0.7630	0.0385	84.862
3	1.316	0.00588	0.00368	0.0118050	0.030348	0.026364	1.00	0.9482	0.58602	0.8719	0.0344	83.881
4	1.340	0.00679	0.00291	0.0138129	0.030610	0.026463	1.02	1.0443	0.54662	0.9690	0.0569	84.940
5	1.086	0.00686	0.00324	0.0106692	0.020523	0.012652	1.12	1.1543	0.57236	1.0122	0.0557	87.719
6	1.140	0.00630	0.00324	0.0094089	0.021695	0.016398	1.30	1.3137	0.64604	1.0870	0.0430	85.729
7	1.121	0.00496	0.00343	0.0075619	0.013872	0.011084	1.10	1.1211	0.61332	0.8599	0.0473	82.506
8	1.329	0.00570	0.00301	0.0105660	0.024676	0.020085	0.88	0.8831	0.53625	0.8842	0.0496	84.328
9	1.268	0.00629	0.00363	0.0115970	0.025594	0.027876	1.06	1.0337	0.64226	1.0057	0.0540	85.751
10	1.181	0.00577	0.00332	0.0089521	0.017828	0.010918	0.98	0.9847	0.51333	0.8095	0.0558	83.277
11	1.186	0.00680	0.00355	0.0100868	0.024225	0.017695	1.12	1.1115	0.60676	1.1757	0.0506	83.943
12	1.258	0.00606	0.00340	0.0103612	0.020306	0.016492	0.92	0.9362	0.53066	0.8464	0.0465	83.437
13	1.189	0.00577	0.00308	0.0093401	0.019894	0.017077	1.26	1.2589	0.60744	1.0274	0.0686	83.731
14	1.116	0.00488	0.00290	0.0070443	0.005470	0.003350	0.80	0.8550	0.346227	0.5505	0.0881	85.825
15	1.153	0.00593	0.00276	0.0103535	0.021464	0.018206	1.20	1.2684	0.621714	1.1423	0.0591	85.595
16	1.098	0.00623	0.00353	0.0095051	0.013708	0.017651	1.44	1.4431	0.687611	1.1243	0.0521	83.651
17	1.254	0.00702	0.00374	0.0113310	0.022404	0.020627	1.06	1.0509	0.552263	0.9281	0.0781	84.968
18	1.092	0.00585	0.00324	0.0084073	0.022703	0.020161	1.32	1.2865	0.792187	1.3149	0.0677	83.620
19	1.109	0.00531	0.00340	0.0092397	0.016459	0.006652	1.16	1.1304	0.427236	0.6429	0.0373	85.404
20	1.084	0.00547	0.00298	0.0069416	0.018299	0.009675	1.36	1.3545	0.686052	1.0320	0.0689	82.235
Mean	1.194	0.00598	0.00324	0.0099303	0.020224	0.016546	1.10	1.1029	0.5757	0.9487	0.05520	84.497
SD	0.087	0.00058	0.000297536	0.0016384	0.005623	0.006233	0.17	0.1663	0.0966	0.1774	0.01331	1.271
CV	0.07266	0.0964	0.0918	0.164993	0.27802	0.37673	0.154	0.1508	0.1678	0.1869	0.2411	0.015039

### 3.2. Deflection and flexural rigidity

The stem deflection used to calculate EI is shown in Figure 7. All deflections tested are shown in Figure 7. Each geometrical shape indicates a result of the deflection test conducted for 60 cases. When the stems were loaded with 3.0 g, the average EI was  $\sim 0.016 \text{ Nm}^2$ .

Numerical data and deflection wave measurements are shown in Figure 8. For the models, the deflection curves were plotted through nodes in the centroid of each cross-section, and markers are shown at every 100 nodes in Figure 8. Number of elements was 13,832 in both models.

From the measurements, stem deflection was smaller around its base and larger around its top than in the other regions. For Model B with a truncated trigonal pyramidal shape, its deflection was small around its base, in consistency with the measured values because its EI value was the maximum at  $y = 0$ . Model A had fixed EI values along the stem. These deflections around the base and at the top became larger than the measurement and Model B.

### 3.3. Forced frequency response

There was a sharp peak at 0.98 Hz, as  $f$ , with the amplitude ratio, changed within 0.2 Hz in the peak in the forced frequency response curve (Figure 9). The amplitude ratio was defined as the ratio of vibration stroke to amplitude at the top of the swinging stem. Before 3.0 Hz, which was the maximum frequency used in this study, the amplitude ratio increased again.

### 3.4. Free damping response curve

The average damping coefficient in this study was 0.05520.  $f_D$  was calculated using Equation 5 with  $\xi$ . When there was no external force in the experiment, the analytic solutions

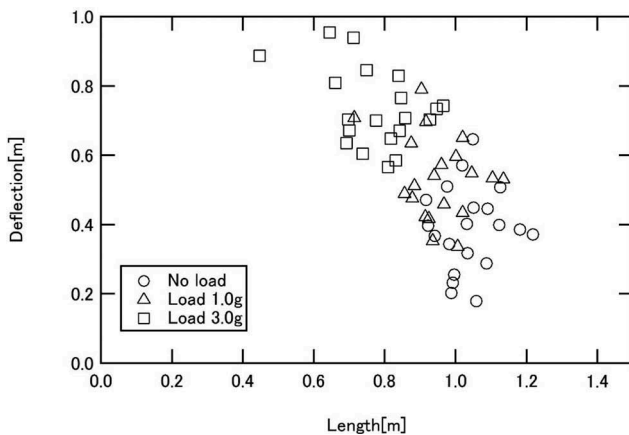


Figure 7. The deflection of the *C. malaccensis* stem. All deflections tested are shown in the figure. Each geometrical shape indicates a result of the deflection test conducted for 60 cases.

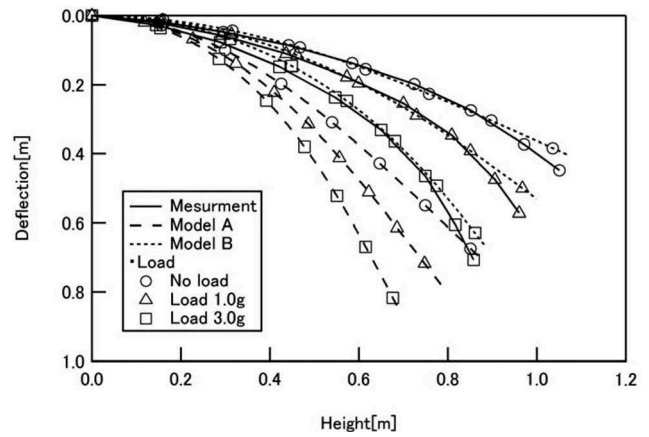


Figure 8. Deflection curves for measurements and finite element models of sample No. 1. For the models, the deflection curves were plotted through nodes in the centroid of each cross-section, and markers are shown at every 100 nodes in the figure. The number of elements was 13,832 in both models.

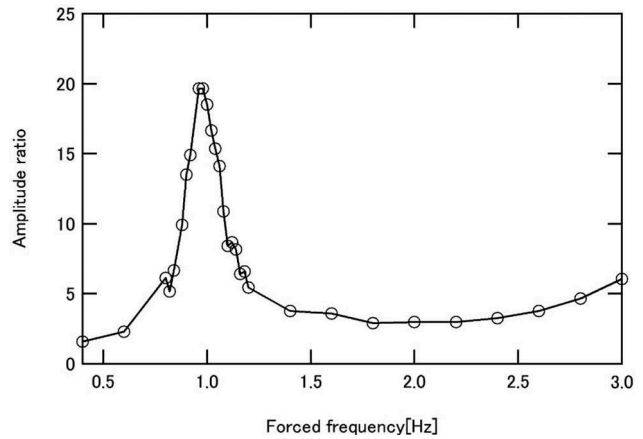
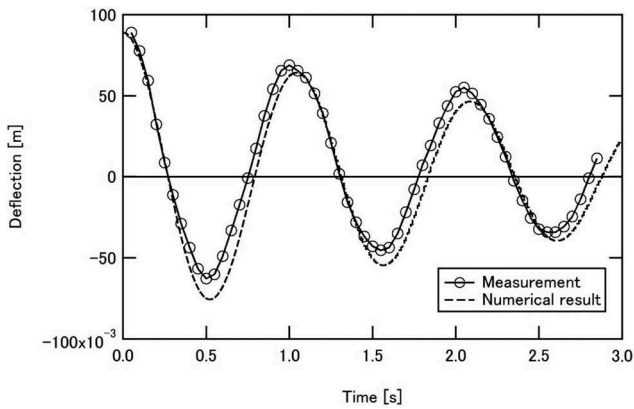


Figure 9. Frequency response curve plotted using forced frequency. The amplitude ratio was defined as the ratio of vibration strokes to amplitude at the top of the swinging stem. The forced frequency was increased by 0.02 Hz from 0.8 Hz to 1.0 Hz and 0.2 Hz in another and measured using sample No. 1.

and numerical values calculated using  $f_D$  and  $\xi$  corresponded (Figure 10). Displacement was measured using sample No. 1. The analytical solution was achieved by solving Equation 5, and numerical data were obtained using the Newmark- $\beta$  method. The measured damping response was consistent with these solutions.

### 3.5. Comparison of natural frequencies

The average values of  $f$ ,  $f_D$ ,  $f_A$ , and  $f_B$  are presented in Table 1.  $f_D$ , calculated using the natural damping response, was consistent with  $f$ , calculated using the forced frequency response. Based on the numerical



**Figure 10.** Damping response of sample No. 1. Displacement was measured using sample No. 1. The numerical data were obtained using the Newmark- $\beta$  method.

solution, the natural frequencies calculated using both finite element models were smaller than the measured values, and  $f_{A_r}$ , calculated with the triangular prism model, was smaller than  $f_{B_r}$ , calculated with the truncated trigonal pyramid model.

#### 4. Discussion

Based on the side lengths of the cross-sections, the *C. malaccensis* stem was established to be tapered, because  $d_t$  was approximately one-half of  $d_b$ .

Considering the stem as a flat cantilever beam in Equation 2,  $EI$  was calculated irrespective of  $L$ . When the models used in this study had the same  $L$  and  $EI$ , the deflection of Model A became larger than that of the measurement and Model B because the deflection at the top was maximum when the model was flat and not tapered. When  $E$  was fixed in a model, with tapered shape, the measurement and numerical solution obtained using a model were observed to closely correspond with each other.

Based on the modal analysis, Model A had a lower frequency than Model B. Natural frequency generally decreases as the beam becomes longer and more flexible. It suggested that the deformation of Model A was easier than that of the tapered model when these models had the same length. This finding was compatible with model deflection.

By comparing flexural rigidity values between the stems and rice stalks, whose  $EI$ , length, and water content were  $0.0215 \text{ Nm}^2$ , 560 mm, and was 65.9%, respectively (Inoue et al., 1998), the stems were observed to be more flexible than rice stalks.

The extinction of the second vibration mode was predicted by the re-increase in amplitude ratio. The average natural frequency of rice stalks was reported

to be 1.09 Hz (Inoue, Hirai & Hashiguchi et al., 2000). The stiffness of *C. malaccensis*, whose stem was approximately twice as long as that of rice, was suggested to cause the natural frequencies of its stem and rice stalks to be close to each other. This suggestion corresponded with the flexural rigidity values.

The damping coefficients of alfalfa and wheat were 0.0875 and 0.0859, respectively (Martines-Vazquez & Sterling, 2011). The *C. malaccensis* stem had smaller damping coefficients than these plants, and it was easier to continue swinging.

By comparing the measured and calculated damping curves, it was suggested that the damping response could be estimated using natural frequency and damping coefficient if plant stems are tapered, similar to *C. malaccensis* stems.

In this study, the flexural rigidity, natural frequency, and damping coefficient of *C. malaccensis* were measured. These parameters were evaluated by numerical calculation. The results of this study are as follows:

- (1) Flexural rigidity was calculated using measured deflection. Its average was  $0.016 \text{ Nm}^2$  when *C. malaccensis* stem was loaded with 3.0 g.
- (2) Natural frequency was calculated using the amplitude ratio from the forced vibration experiment, and its average was 1.10 Hz.
- (3) By calculating the numerical values of deflection and natural frequency using the FEM with Young's modulus, the results of the triangular prism model were more different from the measurements than were the results of the truncated trigonal pyramid model from the measurement. These suggested characteristics of *C. malaccensis* were affected by the shape of the finite element models.
- (4) Damping coefficient was calculated using the free vibration response. The measured damping curve was consistent with the analytical solution and numerical data.

These characteristics evaluated in this study are useful in simulating the motion of *C. malaccensis* in cultivated fields.

#### Acknowledgments

The authors would express their appreciation to Mr. Takahiro Sugita and Ms. Tomoyo Oka for their help in measuring property of *Cyperus malaccensis* Lam.

#### Disclosure statement

No potential conflict of interest was reported by the authors.

## References

- Baker, C. J. (1995). The development of a theoretical model for the windthrow of plants. *Journal of Theoretical Biology*, 175, 355–372.
- Cultivated Soil Classification Committee. (1995). Classification of cultivated soils in Japan (third approximation). *Miscellaneous Publication of the National Institute of Agro-Environmental Sciences*, 17, 1–79. Japanese.
- Dupont, S., Gosselin, F., Py, C., Delangre, E., Hemon, P., & Nurunet, Y. (2010). Modelling waving crops using large-eddy simulation: Comparison with experiments and a linear stability analysis. *Journal of Fluid Mechanics*, 652, 4–44.
- Flesch, T. K., & Grant, R. H. (1992). Corn motion in the wind during senescence: II. Effect of dynamic plant characteristics. *Agronomy Journal*, 84, 748–751.
- Hanawa, T., Miyauchi, S., Takeuchi, S., & Kajishima, T. (2015). DNS analysis of the interaction between turbulent flow and elastic fibers implanted on a flat plate, *9th International Symposium on Turbulence and Shear Flow Phenomena, Melbourne, Australia*, 9A-4.
- Hayashi, H. (2014). Kunisaki Peninsula Usa integrated forestry, agriculture and fisheries system, which is one of the globally important agricultural heritage systems (GIAHS), Values Shichitoui (*Cyperus malaccensis* Lam.) by the devoted cooperation from regional agricultural experimental stations. *Fertilizer Science*, 36, 1–25. Japanese.
- Inoue, E. (1963). On the turbulent structure of airflow within crop canopies. *Journal of the Meteorological Society of Japan*, 41, 314–326.
- Inoue, E., Hirai, Y., Hashiguchi, K., & Okayasu, T. (2000). Frequency response characteristics of rice stalk. *Journal of the Japanese Society of Agricultural Machinery*, 62, 73–80. Japanese.
- Inoue, E., Kim, Y., Hashiguchi, K., Okayasu, T., & Kashima, J. (1998). Mechanical characteristics of rice stalk. *Journal of the Japanese Society of Agricultural Machinery*, 60, 97–102. Japanese.
- Karamchand, K. S., Sridhar, K. R., & Bhat, R. (2009). Diversity of fungi associated with estuarine sedge *Cyperus malaccensis* Lam. *Journal of Agricultural Technology*, 5, 111–127.
- Martines-Vazquez, P., & Sterling, M. (2011). Predicting wheat lodging at large scales. *Biosystems Engineering*, 109, 326–337.
- Murakami, T., Harazono, Y., Kawamura, R., & Nishizawa, T. (1990). The interaction of turbulent air flow and communities of rice plants and red-pines. 2. Characteristics of turbulent transport over canopies caused by plant swaying. In *Bulletin of environmental research center, the University of Tsukuba* (pp. 15–29).
- Newmark, N. M. (1959). A method of computation for structural dynamics. *Journal of Engineering Mechanics*, 85, 67–94.
- Vogel, S. (1984). Drag and flexibility in sessile organisms. *American Zoologist*, 24, 37–44.